ARTICLES

Energy-Dependent Quantum-State-Resolved Relaxation of Highly Vibrationally Excited Pyridine (E_{vib} = 36 990−40 200 cm^{-1}) through Collisions with CO_2

Jeunghee Park, Ziman Li, Andrew S. Lemoff, Craig Rossi, Michael S. Elioff, and Amy S. Mullin*

Department of Chemistry, Arthur G. B. Metcalf Center for Science and Engineering, Boston University, Boston, Massachusetts 02215

Received: June 13, 2001; In Final Form: January 31, 2002

The energy dependence of "strong" collisional deactivation that transfers energy from highly vibrationally excited pyridine to a CO_2 bath has been investigated for pyridine with internal energy between E_{vib} = 36 990 and 40 200 cm^{-1}. Highly excited pyridine was prepared by absorption of tunable pulsed UV laser light at four wavelengths, λ = 251, 259, 266, and 273 nm, followed by prompt radiationless decay from S_1 (or S_2) to the vibrationally excited levels of the ground electronic state. High-resolution transient IR absorption spectroscopy was used to measure the nascent rotational and translational energy distributions of scattered CO_2 molecules in high J states of the ground vibrationless (00^00) level that result from collisions with hot pyridine. Our results reveal that substantial amounts of rotational and translational energy are imparted to CO_2(00^00) molecules for all four pyridine energies and that the magnitude of the CO_2 rotational and translational energy gains changes very little for a 3000 cm^{-1} change in the vibrational energy of the pyridine donor. State-resolved energy-transfer rate constants were measured at each UV wavelength and were also found to be fairly insensitive to changes in the donor internal energy content for the excitation energies studied here. These results indicate that the relaxation mechanism and the energy-transfer probability distribution function for the V → RT pathway for pyridine(E)/CO_2 collisions are invariant to this change in internal energy. A consideration of energy-transfer rates using Fermi's Golden Rule is consistent with the observed behavior. Comparison with previous energy-dependent collisional quenching studies [Elioff, M. S.; Wall, M.; Lemoff, A.; Mullin, A. S. *J. Chem. Phys.* **1999**, *110*, 5578−5588] on vibrationally hot pyrazine with CO_2 suggests that this may be a general phenomenon in the collisional relaxation of highly excited molecules.

1. Introduction

High-resolution transient IR absorption studies have revealed that the relaxation of highly vibrationally excited molecules such as pyrazine,[1,2] pyridine,[3] the corresponding methylated azabenzenes,[4,5] and C_6F_6[6] in a CO_2 bath involves "strong" collisions, which impart large rotational and translational energy gains to CO_2 molecules in their ground vibrationless (00^00) state. Single quenching collisions of hot pyrazine containing $E_{vib} \approx$ 40 000 cm^{-1} have been observed that transfer substantial amounts of energy to CO_2, in some instances as much as 8000 cm^{-1}. Although these "supercollisions" occur very infrequently, they remove so much energy that they are an important component of the energy-transfer dynamics that should be taken into account when considering the molecular-energy budget in combustion and atmospheric environments. This type of energy transfer is dominated by impulsive collisions that are mediated through short-range repulsive intermolecular forces and accounts for the high-energy tail of the energy-transfer probability distribution function, which must evolve as a function of donor internal energy according to the conservation of energy. The goal of this study is to explore the ways in which the strong collisions, that is, the energy-transfer encounters with ΔE > 2000 cm^{-1}, are influenced by systematic increases in the donor internal energy. In this paper, we report on the energy-dependent behavior of the large ΔE collisions in the collisional relaxation of highly excited pyridine, C_5H_5N, in a CO_2 bath using high-resolution transient absorption probing of energy gain in the CO_2 bath.

The first energy-dependent state-resolved studies on strong collisional relaxation from our lab focused on collisions of highly vibrationally excited pyrazine (E_{vib} = 31 000−41 000 cm^{-1}) by CO_2.[7] These studies measured the rotational and translational energy content of the scattered CO_2 molecules with E_{rot} > 1350 cm^{-1} (J = 58) as a function of pyrazine internal energy. We found that the rotational and translational energy gain in CO_2(00^00) does not increase smoothly as the donor energy is increased from E_{vib} = 31 000 to 41 000 cm^{-1}, as might be extrapolated from bulk energy loss measurements. Instead, we observe energy-independent plateaus in the amount of energy gain in CO_2 rotation and translation for pyrazine energies of E_{vib} = 31 000−35 000 cm^{-1} and E_{vib} = 37 000−41 000 cm^{-1}. We see an unexpected threshold in both the energy-gain magnitudes and cross section near $E_{vib} \approx$ 36 000 cm^{-1}. For pyrazine with vibrational energy above 36 000 cm^{-1}, the amount of energy imparted to CO_2 rotation increases by ∼25% and the recoil energy increases by as much as 80% for the highest J

10.1021/jp012270p CCC: $22.00
Published on Web 03/15/2002

states studied. In addition, the probability for the large ΔE collisions exhibits a slight energy dependence for $E_{vib} < 37\,000$ cm^{-1}. The collision number Z for this pathway goes from 84 to 50 as pyrazine E_{vib} goes from 31 000 to 37 000 cm^{-1}. At higher pyrazine internal energies, the probability increases sharply, with $Z = 15$ at $E_{vib} = 41\,000$ cm^{-1}. The reasons for the observed threshold are not fully understood at this time, but there is kinetic evidence that the stepwise increase in the strong collision channel is correlated with the dissociation energy of pyrazine.[8,9]

In this paper, we explore this issue by investigating the energy dependence of the large rotational and translational energy-gain channel in CO_2 following collisions with highly excited pyridine with the vibrational energy between 36 990 and 40 200 cm^{-1}. The collisional quenching of pyridine at one internal energy, $E_{vib} = 37\,950$ cm^{-1}, has already been reported. The excitation energy range in this study is limited on the low-energy side by the onset of the UV absorption for pyridine near $\lambda = 275$ nm and on the high-energy side by the availability of shorter UV wavelengths. Our experiments use the transient diode laser absorption technique originally developed by Flynn and coworkers,[10] combined with tunable UV excitation, to study how the donor energy influences the various energy-transfer pathways. Highly vibrationally excited pyridine molecules with vibrational energy $E_{vib} = 36\,990-40\,200$ cm^{-1} are prepared by pulsed tunable UV with four distinct wavelengths, $\lambda = 251$, 259, 266, and 273 nm. The band origin of the S_0-S_2 transition is at $\lambda = 260$ nm; pyridine is initially excited to the S_1 state at $\lambda = 273$ and 266 nm and to the S_2 state at $\lambda = 259$ and 251 nm.[11] Following optical excitation, pyridine subsequently undergoes fast internal conversion to highly vibrationally excited levels of the ground electronic state, with reported S_1 and S_2 lifetimes of $\tau(S_1) = 60$ ps and $\tau(S_2) = 1.3$ ps.[12,13] Thus, the electronic character of the highly excited pyridine at the wavelengths ranging from 273 to 251 nm is essentially S_0 in nature at our data acquisition time of $t = 1$ μs. Scattered CO_2 molecules that are excited through collisions with the hot pyridine donors are probed using high-resolution transient IR absorption spectroscopy, which allows us to probe the energy gain in CO_2 vibration, rotation, and translation. Thus, we are able to identify specific pathways of energy transfer and, through measurements of absolute rate constants, quantify the contributions of individual pathways to the overall collisional relaxation process.

We begin with a description of our experimental methods. We then present our findings on Doppler-broadened line widths and rotational-state populations for the scattered $CO_2(00^00)$ molecules in high rotational states ($J = 60-78$), followed by the rate constants for energy gain into specific CO_2 rotational states. These findings are then discussed in terms of how the internal energy content of hot pyridine influences the statistical distribution of that energy among pyridine's vibrational modes. Finally, we consider the role that the density of states has on the quenching dynamics and invoke Fermi's Golden Rule to relate our experimental probability functions to changes in the density of states.

II. Experimental Section

All of the experiments described here were performed using a transient infrared absorption spectrometer coupled to a tunable pulsed UV laser system, each which has been described previously.[3,14] The spectrometer consists of a 3-m flowing gas collision cell, a high-resolution infrared diode laser, and a pulsed tunable UV laser system. A 1:1 mixture of pyridine and CO_2 was allowed to flow through a 300.5-cm (1 in. diameter) Pyrex cell maintained at a total pressure of 20 mTorr at $T = 298$ K. Pulsed UV light was generated using the frequency-tripled output of a tunable 10 Hz Nd:YAG pumped Ti:sapphire laser ($\lambda = 251-273$ nm) resulting in vibrationally excited pyridine molecules with $E_{vib} = 36\,990-40\,200$ cm^{-1}). The UV output had a pulse width of $\tau \approx 5$ ns. The UV power density for all experiments was maintained below 1 MW/cm^2 to minimize the effects of multiphoton absorption.

Rotationally excited populations of scattered $CO_2(00^00)$ molecules were probed using a liquid-nitrogen-cooled cw infrared ($\lambda = 4.3$ μm, 200 μW) diode laser with a resolution of 0.0003 cm^{-1}. The IR beam was propagated collinearly with the UV excitation beam through the collision cell and the transmitted IR intensity was passed through a monochromator, collected on a liquid-nitrogen-cooled InSb detector, and amplified using a matched amplifier with a rise time of $\tau < 300$ ns. The resulting transient absorption signals were sent to a digital oscilloscope and transferred to a computer for analysis. Typically, transient absorption signals were averaged for 300−500 UV laser pulses at a repetition rate of 1 Hz.

The IR diode laser frequency was controlled in these experiments using active feedback stabilization. For population measurements, roughly 10% of the IR laser was split off the main IR beam and steered through a 120-cm CO_2 reference cell and onto a second InSb detector. The output was amplified and directed into a lock-in amplifier, which actively corrected for drifts in the diode laser current. This setup allowed us to lock the diode laser optical frequency to the center of a single rovibrational transition of CO_2.

Doppler-broadened line profiles provide a measurement of the translational-energy content of the scattered molecules. Transient Doppler profiles for individual CO_2 rotational states were acquired by replacing the reference cell with a scanning Fabry−Perot etalon. Doppler line widths were obtained by locking the diode probe frequency onto an etalon fringe and acquiring transient absorption intensities at ~40 distinct frequencies over a ~0.04 cm^{-1} range centered on a CO_2 absorption line of interest. Prior to each line width measurement, the voltage used to scan the etalon was calibrated by scanning between two nearby well-known CO_2 transitions. All population measurements were acquired at $t = 1$ μs after the UV pulses and were collected as a function of infrared frequency from the center of the absorption peak. The average time between collisions for a pyridine/CO_2 mixture at 298 K is $\tau_{col} \approx 4$ μs, so by collecting transient absorption signals at 1 μs, we can minimize undesirable relaxation effects due to secondary collisions.

A dual signal technique is used to collect transient absorption signals to minimize effects due to fluctuations in infrared laser intensity. The quantity in which we are interested is the fractional absorption or $\Delta I/I_0$. Beer's law gives us the expression

$$\frac{\Delta I}{I_0} = 1 - \exp[-\alpha p l] \qquad (1)$$

where α is the absorption coefficient for an individual CO_2 state, derived from the HITRAN database[15] absorption strength, p is the population of that state, and l is the path length.

Rotational population distributions for scattered CO_2 molecules were collected using a rotational reference technique to account for fluctuations in UV power, cell pressure, and temperature. Transient absorption measurements for individual rotational states are measured relative to one state that acts as a population reference. The pairs of relative rotational populations are then scaled to a single value for the reference state,

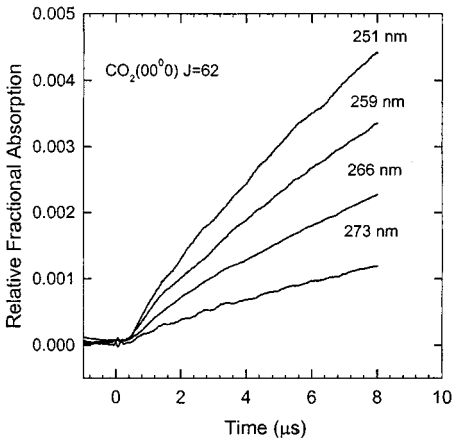

Figure 1. Transient absorption signals for $CO_2(00^00)$ $J = 62$ following collisions with vibrationally excited pyridine (E_{vib} = 40 200, 38 790, 37 950, and 36 990 cm^{-1}). The vibrationally hot pyridine is prepared using 251, 259, 266, and 273 nm electronic excitation, followed by radiationless decay to the ground electronic state. The total cell pressure is 20 mTorr at $T = 298$ K, and the average gas kinetic collision time is $\tau_{col} \approx 4$ μs.

resulting in a more accurate measurement of the rotational population distribution.

Prior to use, pyridine (C_5H_5N, Aldrich, 99+%) was fractionally distilled, degassed through multiple freeze/pump/thaw cycles, and stored over molecular sieves. Research-grade CO_2 (Matheson, 99.995% purity) was used without further purification. For the reference cell, CO_2 (Northeast Airgas, 99.8% purity) was used without further purification.

III. Results

A. Energy-Dependent Transient Absorption Measurements. The appearance of $CO_2(00^00)$ molecules in high rotational states, $J = 60-78$, resulting from collisions with highly vibrationally excited pyridine was measured for ~ 10 μs following the UV excitation of pyridine, using the diode laser transient absorption spectrometer. The IR probe transition involves excitation of one quantum of the strongly allowed ν_3 antisymmetric stretching mode at 2349 cm^{-1},

$$CO_2(00^00,J,V) + h\nu\ (\lambda \approx 4.3\ \mu m) \rightarrow CO_2(00^01,J\pm1,V) \quad (2)$$

where J is the rotational quantum number, and V is the velocity component parallel to the diode laser propagation axis for the scattered CO_2 molecules. Transient absorption profiles for $CO_2(00^00, J = 62)$ following collisions with pyridine excited at the wavelengths $\lambda = 251$, 259, 266, and 273 nm are shown in Figure 1. The mean time between collisions in the gas sample is $\tau_{col} \approx 4$ μs under our experimental conditions. This is much longer than the detector rise time of 300 ns so that the amplitude of the rise corresponds to the population change for an individual rovibrational state. The number density for individual rotational states of CO_2 was determined from the change in the fractional IR absorption using Beer's law and well-established CO_2 absorption cross sections. Transient absorption data such as those presented in Figure 1 were used to determine the nascent rotational and translational energy distributions of the scattered CO_2 molecules, as described in the next sections. Population measurements were determined at $t = 1$ μs following the UV pulse so that population changes correspond essentially to single encounters between vibrationally hot pyridine and CO_2.

B. Energy-Dependent Translational Energy Gain in $CO_2(00^00)$. Doppler-broadened line shapes for a number of individual $CO_2(00^00)$ rotational states were measured at $t = 1$ μs following UV excitation of pyridine to determine the distributions of recoil velocities that accompany energy gain into $CO_2(00^00)$ rotational states $J = 60-78$. Transient line shape measurements were collected as a function of pyridine internal energy at excitation wavelengths of $\lambda = 251$, 259, 266, and 273 nm. Transient line shapes for $CO_2(00^00)$ $J = 74$ are shown in Figure 2, following pyridine excitation with these four wavelengths. Each data point, represented by a circle, results from an average of 350−500 transient absorption measurements. The data fit well to a Gaussian function represented by the solid line. Assuming an isotropic velocity distribution, the nascent translational temperatures associated with scattering of individual rotational states of $CO_2(00^00)$ were determined from Doppler broadened full width at half-maximum line widths. The line widths for $CO_2(00^00)$ $J = 74$ are significantly broadened relative to the initial CO_2 line width of 0.0043 cm^{-1} at 298 K and correspond to the lab frame translational temperatures $T_{trans} = 1830-2040$ K for the four pyridine energies. Conversion to the center-of-mass (as described previously[14] and in Table 1) yields relative translational temperatures $T_{trans}(com) = 2680-3020$ K for $J = 74$. Transient line width data for a number of high J states of $CO_2(00^00)$ and their corresponding translational temperatures, both in the lab frame and center-of-mass frame, are listed in Table 1. At the excitation wavelength $\lambda = 266$ nm, we have already reported the line widths for $CO_2(00^00)$ $J = 60-78$, which are consistent with the values presented in Table 1 within the experimental error.[3]

Values of $T_{trans}(com)$ are plotted in Figure 3 as a function of final CO_2 rotational state energy for pyridine excitation wave-

TABLE 1: Transient Absorption Linewidths and Translational Temperatures of $CO_2(00^00)$ Rotational States Resulting from Collisions with Highly Vibrationally Excited Pyridine, Pyridine(E_{vib}) + CO_2 → Pyridine($E_{vib}-\Delta E$) + $CO_2(00^00,J)$

pyridine E_{vib} (cm^{-1})	J	$\Delta\nu_{obs}$ (cm^{-1})[a]	T_{trans}(lab)[b] (K)	T_{trans}(com)[c] (K)
40 200	60	0.0079	1010 ± 202	1408 ± 315
	66	0.0082	1109 ± 222	1561 ± 345
	68	0.0090	1336 ± 267	1914 ± 416
	70	0.0097	1539 ± 308	2230 ± 479
	74	0.0109	1972 ± 394	2904 ± 614
	78	0.0118	2321 ± 464	3448 ± 723
38 970	60	0.0081	1076 ± 237	1509 ± 369
	66	0.0085	1189 ± 262	1685 ± 407
	70	0.0096	1523 ± 335	2205 ± 522
	74	0.0105	1829 ± 403	2682 ± 627
	78	0.0122	2481 ± 546	3697 ± 850
37 950	66	0.0081	1080 ± 259	1515 ± 404
	74	0.0110	2008 ± 481	2961 ± 750
	78	0.0120	2400 ± 576	3571 ± 897
36 990	60	0.0076	952 ± 248	1317 ± 386
	62	0.0082	1110 ± 289	1562 ± 449
	66	0.0085	1192 ± 310	1690 ± 482
	70	0.0098	1597 ± 415	2320 ± 646
	74	0.0111	2045 ± 531	3018 ± 828
	78	0.0115	2204 ± 573	3266 ± 892

[a] Full width at half-maximum line widths from transient absorption line width at 1 μs following pyridine excitation. Line widths are reported to within ±0.001 cm^{-1}. [b] Lab frame translational temperatures are determined using $T_{trans} = (mc^2/(8R \ln 2))(\Delta\nu_{obs}/\nu_0)^2$, where m is the mass of CO_2, c is the speed of light, R is the gas constant, $\Delta\nu_{obs}$ is the full width at half-maximum line width of the fitted transient line shape, and ν_0 is the center frequency of the absorption line. [c] Center-of-mass translational temperatures, $T_{trans}(com)$, are calculated using $T_{trans}(com) = T_{trans}(lab) + (T_{trans}(lab) - T_{cell})(m_{CO_2}/m_{pyd})$, where $T_{trans}(lab)$ is the lab-frame translational energy of CO_2, T_{cell} is the temperature of the collisional cell, and m_{CO_2} and m_{pyd} are the masses of CO_2 and pyridine.

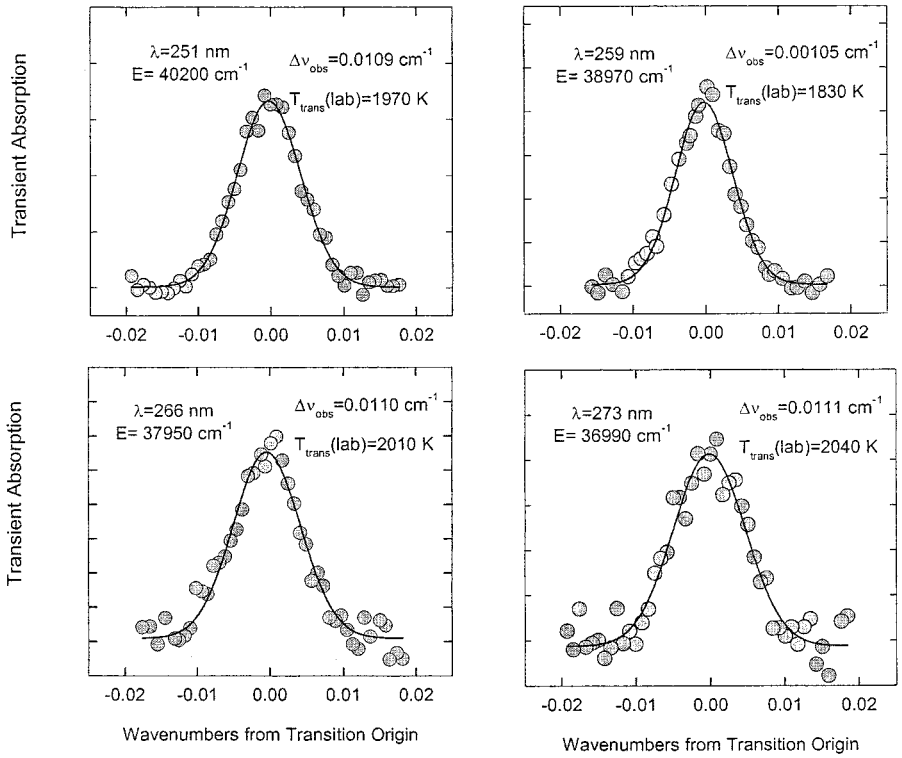

Figure 2. Transient absorption line shapes for $CO_2(00^00)$ $J = 74$ resulting from collisions with vibrationally excited pyridine (E_{vib} = 40 200, 38 790, 37 950, and 36 990 cm^{-1}). Open circles are data collected at 1 μs following UV excitation of pyridine at λ = 251, 259, 266, and 273 nm. The data are fit to a Gaussian function (shown as a solid line), resulting in a full width at half-maximum of $\Delta\nu_{obs}$ as reported in Table 1.

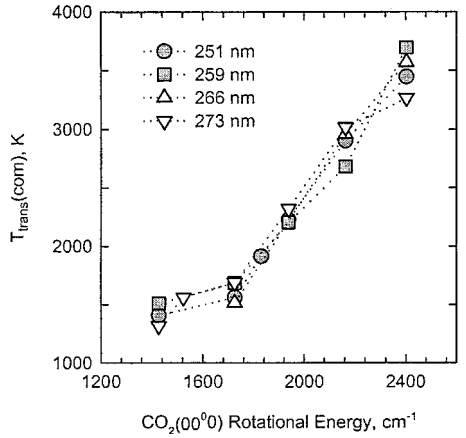

Figure 3. The com (center-of-mass) translational temperature for J = 66, 74, and 78 states of $CO_2(00^00)$, resulting from collisions with vibrationally hot pyridine, collected at 1 μs following pyridine excitation, as a function of pyridine vibrational energy (E_{vib} = 40 200, 38 790, 37 950, and 36 990 cm^{-1}). The dotted line connects the data points as a guide to the eye. For comparison, the room temperature, 298 K, is shown as a dashed line.

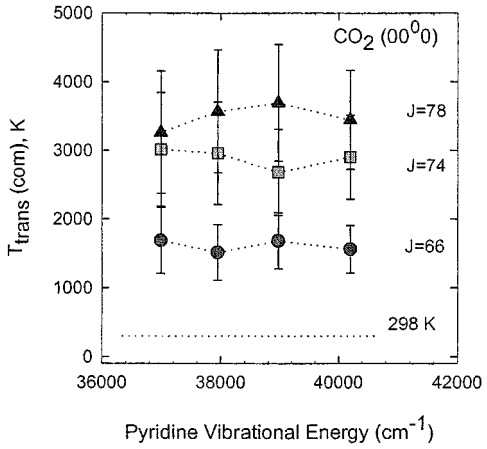

Figure 4. Rotational-state dependence of com translational temperature for high J states of $CO_2(00^00)$, resulting from collisions with vibrationally hot pyridine, collected at 1 μs following pyridine excitation at 251, 259, 266, and 273 nm. There is no apparent energy dependence in the observed line widths, within our experimental error.

lengths λ = 251, 259, 266, and 273 nm. We note that the temperatures increase monotonically as a function of J and have values as high as 3500 K for $CO_2(00^00)$ J = 78. Similar J-dependent T_{trans} data are seen in the quenching of other highly vibrationally excited donor molecules with CO_2, and this behavior is the signature of impulsive collisions with CO_2. It is significant that the translational temperatures follow essentially the same rotational-state dependence, irrespective of the excitation wavelength. In Figure 4, the energy dependence of the T_{trans}(com) over the range of pyridine internal energy is shown for $CO_2(00^00)$ J = 66, 74, and 78, where solid symbols are experimental data points and the dotted lines provide a guide to the eye. There is little change in the translational temperatures of the scattered $CO_2(00^00)$ molecules for any of these high rotational states over the range of pyridine energies E_{vib} = 36 990−40 200 cm^{-1}.

C. Energy-Dependent Rotational-State Distributions of $CO_2(00^00)$ $J = 60-78$. The distributions of rotational states of the scattered $CO_2(00^00)$ molecules with J = 60−78 were measured as a function of pyridine excitation wavelength, λ = 251, 259, 266, and 273 nm. The nascent rotational distributions were obtained from the relative $CO_2(00^00)$ number densities measured at t = 1 μs following pyridine optical excitation, and the data were fit to a Boltzmann rotational distribution, given by $\ln\{[CO_2(00^00,J)]/(2J+1)\} = -BJ(J+1)/(k_BT_{rot})$, using a nonlinear least-squares analysis. Here, $[CO_2(00^00,J)]$ is the number density of scattered CO_2 molecules in the J rotational

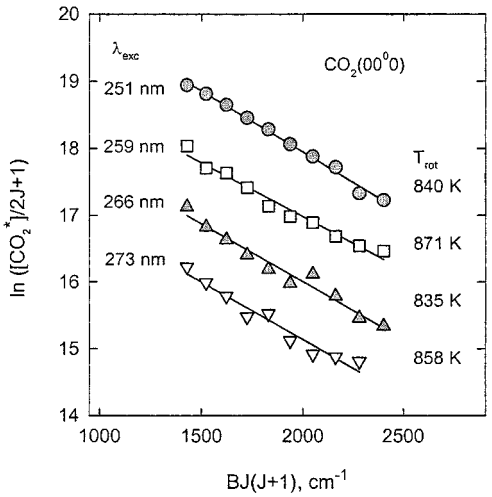

Figure 5. Energy-dependent nascent rotational distributions for $CO_2(00^00)$ $J = 60-78$, resulting from collisions with vibrationally excited pyridine, collected at 1 μs following pyridine excitation ($E_{vib} = 40\,200$, 38 790, 37 950, and 36 990 cm^{-1}). The pyridine internal energies and the resulting T_{rot} values are listed for each distribution. The solid lines are least-squares fits to the CO_2 population data measured at 1 μs following UV excitation of pyridine.

TABLE 2: Nascent Rotational Temperatures for High J States of $CO_2(00^00)$ Resulting from Collisions with Highly Vibrationally Excited Pyridine, Pyridine(E_{vib}) + CO_2 → Pyridine($E_{vib}-\Delta E$) + $CO_2(00^00,J)$

λ_{exc} (nm)	E_{vib} (cm^{-1})	T_{rot} (K)[a]
251	40 200	840 ± 85
259	38 970	871 ± 90
266	37 950	835 ± 90
273	36 990	858 ± 100

[a] Populations of $CO_2(00^00)$ $J = 60-78$ are measured at 1.0 μs following pyridine excitation at a total pressure of 20 mTorr. The data are fit to a Boltzmann distribution, as shown in Figure 5, and the rotational temperature is determined from the slope of the fit.

state, $2J + 1$ is the rotational degeneracy, B is the rotational constant for CO_2 ($B = 0.394$ cm^{-1}), k_B is Boltzmann's constant, and T_{rot} is the rotational temperature that is determined from the fitting procedure. The nascent rotational distributions for $CO_2(00^00)$ $J = 60-78$ are shown in Figure 5, along with the corresponding excitation wavelengths and rotational temperatures. The rotational temperatures are shown in Table 2 with the excitation wavelengths and corresponding pyridine vibrational energies. We find that the distributions of the scattered $CO_2(00^00)$ high J states are well described by rotational temperatures of 840 ± 85 (251 nm), 871 ± 90 (259 nm), 840 ± 90 (266 nm), and 858 ± 100 (273 nm) K. These data show that there is very little change in the amount of rotational energy that CO_2 gains as the pyridine energy is increased from 36 990 to 40 200 cm^{-1}. In our previous quenching study[3] on pyridine excited at $\lambda = 266$ nm, we reported a CO_2 ($J = 60-82$) rotational temperature of $T_{rot} = 1170 \pm 150$ K, which is higher than the present value of $T_{rot} = 840 \pm 90$ K. We suspect that this difference is the result of higher UV fluxes used in the earlier experiments, which led to more pronounced effects of multiphoton absorption. In the work presented here, care has been taken to maintain UV fluences below 1 MW/cm^2, whereas in the previous study, UV power densities were ~5 MW/cm^2.

D. Energy-Dependent Rates of CO_2 Energy Gain. Absolute rate constants for energy gain into the high J states of $CO_2(00^00)$, $J = 60-78$, that result from collisions with highly vibrationally excited pyridine ($\lambda = 251$, 259, 266, and 273 nm) have been measured. The energy-transfer process that results in rotationally and translationally excited $CO_2(00^00)$ molecules can be described as

$$\text{pyd}(E) + CO_2 \xrightarrow{k_2^J} \text{pyd}(E - \Delta E) + CO_2(00^00,J,V) \quad (3)$$

The appearance of CO_2 molecules in the rotational state J resulting from collisions between vibrationally excited pyridine and CO_2 is characterized by a rate constant k_2^J. For short times following the UV excitation of pyridine, the population changes in the $CO_2(00^00)$ state result essentially from collisions between CO_2 and hot pyridine. These changes are expressed as

$$\frac{d[CO_2(00^00,J)]}{dt} = k_2^J[\text{pyd}(E)][CO_2] \quad (4)$$

By measuring the CO_2 populations at early times following UV excitation, both [pyd(E)] and [CO_2] are basically constant according to the method of initial rates. Other energy-transfer processes, such as pyridine self-quenching and relaxation of scattered CO_2 by secondary collisions, will, in general, contribute to the $CO_2(00^00)$ population changes on longer time scales, but their contribution to our measurements is negligible. This is because the average time between collisions (~4 μs) in our experiments is much longer than our measurement time (1 μs) and the population changes that we measure occur in less than ~1/4 of the collision time. Thus, sequential collisional energy transfer events do not impact our early time signals, and by selectively monitoring the excitation of CO_2, our measurements result solely from collisions of hot pyridine with CO_2.

In the current study, we have reduced the intensity of our UV light source so that the excited pyridine concentration is less than 5% of the total concentration. In our earlier study on pyridine relaxation using $\lambda = 266$ nm, self-quenching was included in the kinetic modeling to account for early time curvature in the transient signals. In the earlier studies, the excited pyridine concentration was as much as 20% of the total sample.[3] We now think that the early time curvature was caused by multiphoton absorption of pyridine, and we have reduced the UV fluences to minimize this effect. Under the milder conditions of this study, linear transient absorption signals such as that in Figure 1 are routinely observed. Under the conditions in the current study, eq 4 can be integrated directly and the rate constant can be determined using

$$k_2^J = \frac{\Delta[CO_2(00^00,J)]}{[\text{pyd}(E)]_0[CO_2]_0\Delta t} \quad (5)$$

where $\Delta[CO_2(00^00,J)]/\Delta t$ is the population increase of the $CO_2(00^00,J)$ state during the time period $\Delta t = 1$ μs following UV excitation. This is determined from the transient absorption signal at 1 μs and is integrated over the nascent velocity distribution measured for each final J state, also determined at 1 μs. The initial CO_2 bath concentration, $[CO_2]_0$, is determined by measuring the static IR absorption of a CO_2 rotational state that is populated at room temperature (300 K). The number density of excited pyridine molecules, $[\text{pyd}(E)]_0$, is determined from the number of UV photons absorbed at $t = 0$. The experiments reported here were performed in a regime in which UV absorption is linear with laser power so that the number density of photons absorbed can be converted directly to the number density of excited pyridine molecules. Absolute rate constants for the energy gain into individual rotational states $J = 60-78$ of $CO_2(00^00)$ states, resulting from collisions with

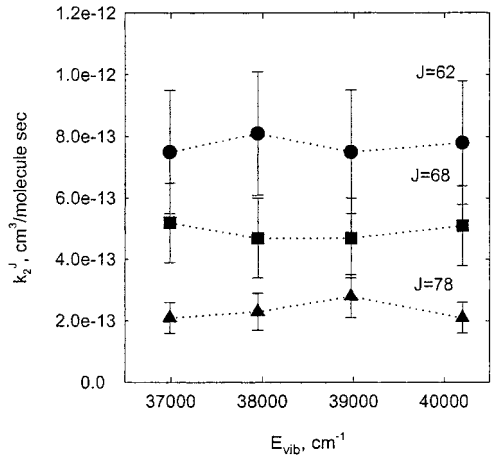

Figure 6. The energy dependence of rate constants for appearance of final rotational states $J = 62$, 68, and 78 of $CO_2(00^00)$, following collisions with pyridine excited at 251, 259, 266, and 273 nm. The observed rates are fairly insensitive to the pyridine internal energy over the range 36 990−40 200 cm^{-1}.

TABLE 3: Absolute Rate Constants, k_2^J, for Energy Gain in $CO_2(00^00)$ Rotational States Resulting from Collisions with Highly Vibrationally Excited Pyridine, Pyridine(E_{vib}) + CO_2 → Pyridine($E_{vib}-\Delta E$) + $CO_2(00^00,J)$

		k_2^J, $\times 10^{-13}$ cm^3 molecule^{-1} s^{-1} *a*			
$CO_2(00^00)$ J	λ_{exc} (nm)	251	259	266	273
	E_{vib} (cm^{-1})	40200	35970	37950	36990
60		8.7 ± 2.2	10.1 ± 2.5	10.6 ± 2.6	9.2 ± 2.3
62		7.8 ± 2.0	7.5 ± 1.9	8.1 ± 2.0	7.5 ± 1.9
64		6.9 ± 1.7	7.2 ± 1.8	6.9 ± 1.7	6.3 ± 1.6
66		5.8 ± 1.4	6.0 ± 1.5	5.7 ± 1.4	4.8 ± 1.2
68		5.1 ± 1.3	4.7 ± 1.2	4.7 ± 1.2	5.2 ± 1.3
70		4.2 ± 1.1	4.1 ± 1.0	4.0 ± 1.0	3.5 ± 0.9
72		3.6 ± 0.9	3.9 ± 0.9	4.6 ± 1.1	3.0 ± 0.8
74		3.1 ± 0.8	3.3 ± 0.8	3.4 ± 0.8	2.9 ± 0.7
76		2.2 ± 0.5	2.9 ± 0.7	2.5 ± 0.6	2.8 ± 0.7
78		2.1 ± 0.5	2.8 ± 0.7	2.3 ± 0.6	2.1 ± 0.5

a All rate constants are determined using eq 5 in the text.

pyridine at the four different UV wavelengths are shown in Figure 6 and listed in Table 3.

To evaluate the overall efficiency of energy transfer into high J states of $CO_2(00^00)$, an integrated rate constant is found by summing over the rate constants for energy gain into individual J states. For this, we define the integrated rate constant as $k_2^{int} = \sum k_2^J$ for $J = 60-78$. The resulting values of k_2^{int} for each UV excitation wavelength are listed in Table 4 and do not change appreciably as the pyridine internal energy increases from 36 990 to 40 200 cm^{-1}. We have also calculated the probability that collisions between excited pyridine and CO_2 will result in $CO_2(00^00)$ $J = 60-78$ by dividing k_2^{int} by the collision rate. Probabilities have been determined using Lennard-Jones and hard-sphere collision rate constants.[16] At $T = 298$ K, the Lennard-Jones collision rate constant is $k_{LJ} = 6.7 \times 10^{-10}$ cm^3 molecule^{-1} s^{-1} and the hard-sphere collision rate constant is $k_{HS} = 3.4 \times 10^{-10}$ cm^3 molecule^{-1}s^{-1}. We find that impulsive collisions between hot pyridine and CO_2 that result in rotationally and translationally excited CO_2 with $J \geq 60$ happen once in 64−72 hard-sphere collisions and once in 127−142 Lennard-Jones collisions for pyridine with $E_{vib} = 36\,990-40\,200$ cm^{-1}.

IV. Discussion

The data presented here demonstrate that the "strong" collisions of vibrationally hot pyridine ($E_{vib} = 36\,990-40\,200$ cm^{-1}) with CO_2 are not exceptionally sensitive to the initial excitation energy of the pyridine. The rotational and translational energy distributions and the energy-transfer cross sections that characterize the scattered $CO_2(00^00)$ molecules in high J states are invariant to the internal energy of pyridine over this range of E_{vib}. For the four excitation wavelengths used in this study, the V → RT energy-transfer channel is characterized by large rotational and translational energy gains in CO_2. The translational temperatures of the scattered $CO_2(00^00)$ molecules with $J = 60-78$ associated with each pyridine excitation energy are very similar, both in magnitude ($T_{trans} \approx 1330-3500$ K) and in their correlation with the final J state, as shown in Figures 3 and 4. The distributions of rotational-energy gain for the high-J $CO_2(00^00)$ molecules are also essentially identical for the four different pyridine vibrational energies, with rotational temperatures of $T_{rot} = 840-870$ K for the $J = 60-78$ rotational states of CO_2. Finally, absolute rate measurements show that this pathway occurs once in ∼135 Lennard-Jones (or ∼70 hard-sphere) collisions, independent of pyridine excitation wavelength.

TABLE 4: Integrated Rate Constants, k_2^{int}, for Energy Gain in $CO_2(00^00)$ $J = 60-78$ Following Collisions with Highly Excited Pyridine, Pyridine(E_{vib}) + CO_2 → Pyridine($E_{vib}-\Delta E$) + $CO_2(00^00,J)$

λ_{exc} (nm)	E_{vib} (cm^{-1})	k_2^{int}, $\times 10^{-12}$ *a* (cm^3 molecule^{-1} s^{-1})	prob$_{LJ}$ *b*	Z_{LJ} *c*	prob$_{HS}$ *d*	Z_{HS} *e*
251	40 200	4.9 ± 1.2	0.0074	136	0.015	69
259	38 970	5.2 ± 1.3	0.0078	128	0.015	65
266	37 950	5.3 ± 1.3	0.0079	127	0.016	65
273	36 990	4.7 ± 1.2	0.0070	142	0.014	72

a k_2^{int} is the integrated rate constant for scattering into the rotationally excited $J = 60-78$ level of $CO_2(00^00)$. *b* The probability to excite $CO_2(00^00)$ $J = 60-78$ through collisions with excited pyridine is defined as k_2^{int}/k_{LJ}. The k_{LJ} is the Lennard-Jones gas kinetic collision rate constant, where $k_{LJ} = \pi[^1/_2(d_{CO_2} + d_{pyridine})]^2\sqrt{8kT/(\pi\mu)}(2\epsilon/(kT))^{1/3}\Gamma(^2/_3) = 6.7 \times 10^{-10}$ cm^3 molecule^{-1} s^{-1} (ref 30) where $d_{CO_2} = 4.50$ Å, $d_{pyridine} = 5.09$ Å, ϵ is the Lennard-Jones well depth (for pyridine $\epsilon/k = 494.7$ K), and Γ is the gamma function. The d and ϵ/k values of pyridine are determined using the critical constants (ref 3). *c* The mean number of Lennard-Jones collisions required to effect the energy transfer into the $CO_2(00^00)$ state, given by $k/_{LJ}k_2^{int}$. *d* The probability to excite $CO_2(00^00)$ $J = 60-78$ through collisions with excited pyridine is defined by k_2^{int}/k_{HS}. The k_{HS} is the hard-sphere gas kinetic collision rate constants given by $k_{HS} = \pi[(d_{CO_2} + d_{pyridine})/2]^2\sqrt{8kT/(\pi\mu)} = 3.4 \times 10^{-10}$ cm^3 molecule^{-1} s^{-1}. *e* The mean number of hard-sphere collisions required to effect the energy transfer into the $CO_2(00^00)$ state, given by k_{HS}/k_2^{int}.

To characterize the amount of energy exchanged in the V → RT quenching of hot pyridine by CO_2, we can use our scattering data to construct an energy-transfer probability distribution function. The procedure for mapping state-resolved scattering probability data into a probability function was first developed by Michaels and Flynn[17] for hexafluorobenzene quenching, and we have since used a similar procedure to characterize other energy-dependent scattering data on pyrazine/CO_2 relaxation.[14] The essential features are as follows. State-resolved energy-gain measurements characterize the *final* rotational states of the scattered CO_2 molecules extremely well, and each rotational level measured has a well-determined velocity distribution. Transformation from the lab to the center-of-mass frame directly yields the distribution of recoil velocities of the scattered donor/acceptor pair, resulting in the distribution of relative translational energies in the scattered molecules. Temperature-dependent scattering data are fit using a gap law to model the energy transfer and provide information about the average *initial*

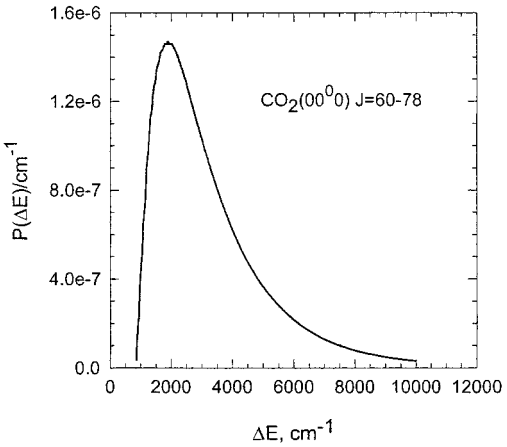

Figure 7. Summed energy-transfer probability distribution function, $P(\Delta E)$, for energy gain ΔE for $CO_2(00^00)$ $J = 60-78$ following collisions with pyridine excited with 251, 259, 266, and 273 nm. This curve corresponds to the V → RT energy-transfer pathway, which is a subset of all possible energy-transfer pathways.

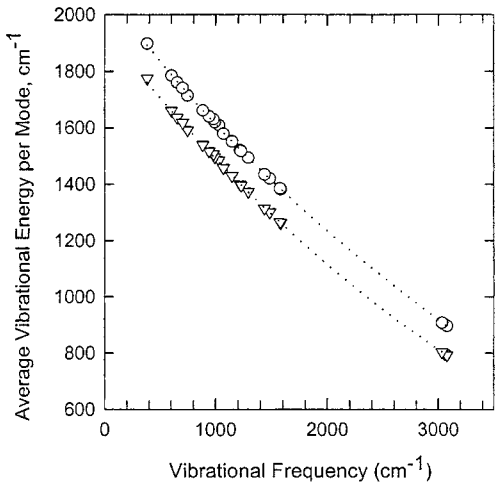

Figure 8. Average vibrational energy residing in individual modes of highly vibrationally excited pyridine prepared with 251 nm (○) and 273 nm (▽) light, calculated using quantum statistics (eq 6).

rotational and translational energies. Thus, the *change* in energy associated with energy transfer resulting in each final CO_2 state is determined. Because our experiments only probe the high J states of CO_2, this approach is useful for obtaining the high-energy portion of the probability function. By taking detailed balance into account, an overall energy-transfer probability distribution function is obtained. The only contribution to the energy-transfer function for this pathway that is not well-characterized in this transformation is the extent of donor internal energy that ends up as rotational energy in the donor. For the quenching of vibrationally hot pyridine with a CO_2 bath, the predominant contributor to the overall probability distribution function for ΔE values greater than 3000 cm^{-1} is the strong collision pathway investigated in this study. This is because vibrational excitation in CO_2 that results from collisions with hot pyridine occurs via long-range energy transfer and is not accompanied by rotational and translational excitation.[3] In this way, the V−V channel is a very narrow feature in the probability function and does not contribute to ΔE values above 3000 cm^{-1}. Similar behavior has been observed for the quenching of vibrationally hot pyrazine and hexafluorobenzene with CO_2 and appears to be a general feature of quenching by CO_2. Therefore, our scattering data, when combined with temperature-dependent measurements, can be directly transformed to a very good approximation into the probability function for large ΔE values. In our analysis of energy-dependent quenching data for hot pyridine and CO_2, we have used the temperature results for pyrazine/CO_2 scattering that the initial CO_2 rotational state is near $\langle J \rangle \approx 28$ and that the initial translational temperature is near 300 K.[2] The summed probability distribution function for the pyridine/CO_2 system obtained from our measurements is shown in Figure 7 for pyridine $E_{vib} = 36\,990-40200$ cm^{-1}. The probability function shown in Figure 7 is most accurate for $\Delta E > 4000$ cm^{-1} because our scattering data begin at $J = 60$ and do not include the translational contributions from lower J states. Our energy-dependent data show that the energy distributions and probabilities for the scattered CO_2 molecules are essentially identical for the different pyridine excitation energies. Thus, the resulting probability distribution functions for each pyridine excitation energy are also the same.

To understand the lack of sensitivity to the initial energy in the donor, we first consider the impact that changes in the energy content of the hot donor have on the distribution of energy among pyridine's vibrational modes. If the internal energy in the hot pyridine is assumed to be statistically distributed, which is reasonable given the large number of modes and the proximity of the vibrational frequencies, then the average energy in each vibrational mode of hot pyridine can be calculated using the following expression:[18]

$$\langle E_{vib} \rangle_i = \frac{h\nu_i \sum_{v_i=1}^{max} v_i \rho_{s-1}(E - v_i h\nu_i)}{\rho_s(E)} \qquad (6)$$

where $\langle E_{vib} \rangle_i$ is the average energy in the ith mode, ν_i is the vibrational frequency of the ith mode, v_i is the summation index over the states in each vibrational mode, max is the maximum quantum number for each mode defined as max $= E/(h\nu_i)$, and ρ_s is the vibrational state density calculated using the Bayer−Swinehart−Stein−Rabinovitch method.[19] The vibrational state densities for pyridine at the internal energies considered in this study are $\rho_s \approx 2 \times 10^{13}$ states per cm^{-1} for $E = 36\,990$ cm^{-1} and $\rho_s \approx 4.3 \times 10^{14}$ states per cm^{-1} for $E = 40\,200$ cm^{-1}. The resulting vibrational energy distributions for the highest and lowest pyridine excitation energies are shown in Figure 8. The distributions for the intermediate excitation energies lie between those shown in Figure 8. We note that the low-frequency modes have the highest populations. It can been seen that, by lowering the internal energy, the average energy per mode is reduced for each mode and that for the range of excitation energies used in this study the average energy per mode decreases by a comparable amount. It is possible that the changes in pyridine energy that we are considering here are not sufficiently large to change the essential nature of the vibrationally hot molecule. For example, the average energy in the lowest frequency mode ($\nu = 380$ cm^{-1}) drops from 1900 to 1770 cm^{-1} when the excitation wavelength goes from 253 to 271 nm, corresponding to average quantum numbers for this mode of 5 and 4.7, respectively. However, this alone does not seem to explain our results for two reasons. One, we have observed a similar lack of energy dependence in the scattering profiles for the large ΔE collisions associated with pyrazine quenching when CO_2 is the bath and pyrazine has $E_{vib} = 31\,000-35\,000$ and $E_{vib} = 36\,990-41\,000$.[7] For this change in excitation energy of the hot donor, the average quantum numbers for the lowest frequency mode ($\nu = 340$ cm^{-1}) change from 4.9 to 6.1. The second reason is that we expect the large ΔE collisions to be

most sensitive tp the energy content in the hot molecule because they involve multiple quanta being transferred in single collisions between the hot donor and the acceptor molecules. In addition, a number of theoretical and experimental studies point to the importance of the low-frequency modes in driving the large ΔE encounters.

An alternate explanation for the apparent lack of energy dependence in our results comes from a consideration of how the density of states in vibrationally hot pyridine changes because of energy loss from collisions with CO_2 molecules and how these collision-induced changes are affected by varying the excitation wavelength that prepares the hot molecule. Collisions of CO_2 and vibrationally hot pyridine move pyridine from a dense manifold of vibrational states at energy E to a less-dense manifold at energy $E - \Delta E$. These energy transfer events simultaneously move CO_2 into higher energy states. Our measurements of energy gain in the CO_2 bath characterize the distributions for the large ΔE impulsive collisions, as shown in Figure 7 in which ΔE values as large as 9000 cm^{-1} are observed. We would like to understand what controls the *shape* of this probability function and its dependence (or lack thereof) on the initial excitation energy. From Fermi's Golden Rule, transition rates from single states to a continuum of states depend on the square of the matrix element, $|V_{if}|$, that couples the initial $|i\rangle$ and final $|f\rangle$ states and on the density of states, ρ, in the continuum.[20] We can extend these ideas to consider the collisional energy transfer from one dense manifold (at energy E) to another (at energy $E - \Delta E$). In this case, the transition rate will depend on the product of the initial and final state densities, $\rho(E)$ and $\rho(E-\Delta E)$, respectively, and for a given impulsive energy-transfer pathway, the matrix element can be taken to be some sort of average over the relevant initial and final states. Thus, for a given impulsive channel, the probability function $P(\Delta E)$ will be proportional to the transition rates associated with those values of ΔE. The transition rate itself is sensitive to the way in which the density of states changes as collisions move the hot pyridine down its vibrational manifold. An important consequence of this is that the energy dependence of the *shape* of the probability function will mimic that of the final density of states, which is determined predominantly by the hot pyridine rather than by the CO_2. The range of energies with which we are concerned here are $E = 36\,990-40\,200$ cm^{-1} and ΔE values from 4000 to 9000 cm^{-1}. We have calculated the harmonic density of states for pyridine using the Beyer−Swinehart−Stein−Rabinovitch[19] algorithm for the energy range 28 000−40 200 cm^{-1}, as shown in the semilog plot in Figure 9. In Figure 9, $\Delta E = 0$ corresponds to pyridine initially excited to $E = 40\,200$ cm^{-1}, and the energy-transfer processes associated with the V → RT pathway studied here correspond to ΔE values between 4000 and 9000 cm^{-1}. The corresponding information for $E = 36\,990$ cm^{-1} is obtained by shifting the abscissa in Figure 9 by 3210 cm^{-1}. If the shape of $P(\Delta E)$ for a given energy-transfer pathway is controlled by the change in the density of states over the range of appropriate ΔE values as predicted by the Golden Rule approach used here, then as long as ρ is exponential in ΔE, the shape of the energy-transfer distribution function will be invariant to changes in excitation energy. It is clear from Figure 9 that for the range of excitation energies used in this study and for the range of ΔE values observed, the density of states is well-described by an exponential function. This prediction is in excellent agreement with our experimental findings for pyridine and pyrazine quenching. In this light, the discontinuity that we observe in the energy-dependent quenching for pyrazine is attributed to an abrupt change in the slope of the density of states, which is consistent with the onset of a dissociative channel. It is worth noting that a similar consideration of the changes in the density of donor states has been extremely successful in describing the shape of the large ΔE probability functions for the quenching of different donor molecules in both CO_2 and H_2O baths. These results are presented elsewhere.[5] It is important to recognize that this approach does not attempt to explain the magnitude of the probability function but merely its shape and the dependence of the shape on the initial excitation energy. The magnitude will be sensitive to the matrix element and the absolute value of the density of states not simply its slope as a function of ΔE. For this, it may be necessary to consider more sophisticated approaches to calculate the density of states.

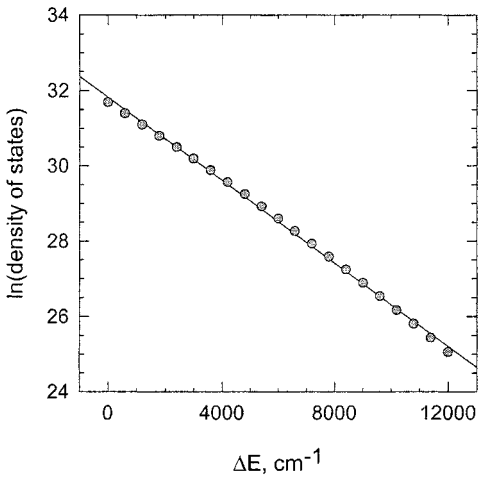

Figure 9. Semilog plot of the harmonic density of states in pyridine initially excited to $E = 40\,000$ cm^{-1} as a function ΔE. The density of states was calculated using the Beyer−Swinehart−Stein−Rabinovitch algorithm.[19] A Golden Rule analysis predicts that the shape of $P(\Delta E)$ for a given energy-transfer pathway will be independent of donor excitation energy as long as the density of states is exponential for the corresponding range of ΔE values.

V. Conclusion

We have performed high-resolution time-resolved experiments to study the energy dependence of the collisional relaxation of highly vibrationally excited pyridine to $CO_2(00^00)$ high J states for the energy range $E_{vib} = 36\,990-40\,200$ cm^{-1}. The nascent rotational and translational energy gains in CO_2-(00^00) corresponding to the high-energy tail of the energy-transfer probability function, $P(\Delta E)$, result from impulsive collisions with ΔE values as large as 9000 cm^{-1}. The energy-gain profiles for the scattered CO_2 molecules exhibit very little dependence on the exact pyridine excitation energy, and the absolute rate constants for this energy transfer pathway are also insensitive to changes in pyridine energy for the range of excitation energies investigated. We interpret these findings using Fermi's Golden Rule to relate the observed probability distribution function to the energy dependence of the density of states for pyridine. This analysis predicts that the shape of the energy-transfer probability function for a given energy-transfer pathway will be invariant to changes in the donor internal energy as long as the density of states is exponential in ΔE, which is in very good agreement with our experimental results. Further studies are underway in our laboratory now to test this idea with other donor/acceptor pairs. Our findings strongly suggest that the nature of the density of states is a controlling factor to the observed relaxation behavior of highly excited molecules and that this type of analysis will lead to the

ability to predict the energy-transfer dynamics in fairly complicated molecular systems.

Acknowledgment. We gratefully acknowledge Professor George Schatz, Professor John Fourkas, and Professor Curt Wittig for fruitful discussions of our data. We also thank E. Korobkova in collecting some of the experimental data. All work was performed at Boston University. This work was supported by the National Science Foundation (Grant CHE-9624533), the Henry Luce Foundation, and the Camille and Henry Dreyfus Foundation, with equipment support from the Office of Naval Research High Energy Density Materials Program (Grant N00014-96-1-0788) and Boston University. A.S.M. was a Clare Boothe Luce Professor (1994−1999) and is a Camille Dreyfus J.P. was supported by the Korea Ministry of Education Foundation (Grant BSRI-99-3432).

References and Notes

(1) Mullin, A. S.; Park, J.; Chou, J. Z.; Flynn, G. W.; Weston, R. E. *Chem. Phys.* **1993**, *175*, 53−70.

(2) Mullin, A. S.; Michaels, C. A.; Flynn, G. W. *J. Chem. Phys.* **1995**, *102*, 6032−6045.

(3) Wall, M. C.; Stewart, B. A.; Mullin, A. S. *J. Chem. Phys.* **1998**, *108*, 6185−6196.

(4) Sevy, E. T.; Rubin, S. M.; Lin, Z.; Flynn, G. W. *J. Chem. Phys.* **2000**, *113*, 4912−4932.

(5) Elioff, M. S.; Fang, M.; Mullin, A. S. *J. Chem. Phys.* **2001**, *115*, 6990−7001.

(6) Michaels, C. A.; Lin, Z.; Mullin, A. S.; Flynn, G. W. *J. Chem. Phys.* **1997**, *106*, 7055−7071.

(7) Elioff, M.; Wall, M. C.; Lemoff, A. S.; Mullin, A. S. *J. Chem. Phys.* **1999**, *110*, 5578−5588.

(8) Michaels, C. A.; Tapalian, H. C.; Lin, Z.; Sevy, E. T.; Flynn, G. W. *Faraday Discuss.* **1995**, *102*, 405−422.

(9) Chesko, J. D.; Stranges, D.; Suits, A. G.; Lee, Y. T. *J. Chem. Phys.* **1995**, *103*, 6290−6292.

(10) Flynn, G. W. *Science* **1989**, *246*, 1009−1015.

(11) Bolovinos, A.; Tsekeris, P.; Philis, J.; Pantos, E.; Andritsopoulos, G. *J. Mol. Spectrosc.* **1984**, *103*, 240−256.

(12) Yamazaki, I.; Murao, T.; Yamanaka, T.; Yoshihara, K. *Faraday Discuss. Chem. Soc.* **1983**, *75*, 395−405.

(13) Yamazaki, I.; Fujita, M.; Baba, H. *Chem. Phys.* **1981**, *57*, 431−440.

(14) Wall, M. C.; Lemoff, A.; Mullin, A. S. *J. Chem. Phys.* **1998**, *102*, 9101−9105.

(15) Rothman, L. L.; Gamache, R. R.; Goldman, A.; et al. *Appl. Opt.* **1986**, *26*, 4058−4098.

(16) Troe, J. *J. Chem. Phys.* **1977**, *66*, 4758−4775.

(17) Michaels, C. A.; Flynn, G. W. *J. Chem. Phys.* **1997**, *106*, 3558−3566.

(18) Durana, J. F.; McDonald, J. D. *J. Chem. Phys.* **1976**, *64*, 2518−2527.

(19) Stein, S. E.; Rabinovitch, B. S. *J. Chem. Phys.* **1973**, *58*, 2438.

(20) Schatz, G. C.; Ratner, M. A. *Quantum Mechanics in Chemistry*; Prentice Hall: Englewood Cliffs, NJ, 1993; p 72.